

Chapter 2

Multifunctional Behavior of TiO₂ Cementitious Composites for Photocatalyst Air Cleaning and Energy Saving



Mona Nazari Sam, Ronald Borges Schiffer, Maximilian Löher, Rodrigo Gibilisco, Jörg Kleffmann, Eduardus Koenders , and Antonio Caggiano 

Abstract Air pollution is still among the biggest environmental health threats for humans in Europe. Traffic, industry, and agriculture are the main responsible sources that are emitting air pollutants, that is, nitrogen oxides (NO_x), sulfur dioxide (SO₂), carbon monoxide (CO), and particulate matter (PM). Moreover, indoor volatile organic compounds (VOCs), such as aromatics, aldehydes, and alcohols, can be emitted by building materials, consumer products, and other sources.

The reduction of these pollutants cannot only be mitigated by active reduction of the emissions but also needs to be mitigated by novel technologies or materials. During the last two decades, novel multifunctional building materials have been designed by embedding photocatalysts employed to reduce (oxidize) the pollutants via photocatalytic reaction (PCR). Photocatalysts, for example, TiO₂, are using UV light to convert adsorbed water and oxygen into highly reactive radicals (OH, O₂⁻), which oxidize (clean) pollutants.

M. N. Sam · R. B. Schiffer · M. Löher · E. Koenders
Institut für Werkstoffe im Bauwesen, Technische Universität Darmstadt, Darmstadt, Germany
e-mail: sam@wib.tu-darmstadt.de; loeber@wib.tu-darmstadt.de;
koenders@wib.tu-darmstadt.de

R. Gibilisco
INQUINOA (CONICET-UNT), Universidad Nacional de Tucumán,
San Miguel de Tucumán, Argentina
e-mail: rgibilisco@fcq.unc.edu.ar

J. Kleffmann
Department of Chemistry and Biology, Bergische Universität Wuppertal,
Wuppertal, Germany
e-mail: kleffman@uni-wuppertal.de

A. Caggiano (✉)
DICCA, Dept. of Civil, Chemical and Environmental Engineering, University of Genova,
Genova, Italy
e-mail: antonio.caggiano@unige.it

In this context, the present work reports recent developments and future trends on experimental and numerical research of employing a multifunctional (highly porous) concrete foam, produced at the Institute of Construction and Building Materials of the *Technische Universität Darmstadt*, and enhanced with embedded TiO_2 . A wide range of experimentally analyzed thermal energy storage outputs, combined with the study of the photocatalytic activity, measured at the *Bergische Universität Wuppertal*, are presented to demonstrate the promising and outstanding multifunctionality of TiO_2 foams.

Keywords Concrete foam · NO_x cleaning · TiO_2 · Multifunctional composites · Photocatalysts

2.1 Introduction

According to the World Health Organization (WHO), air pollution possesses the sixth place among the leading causes of death globally [1]. Traffic, industry, and agriculture are the main responsible sources that are emitting air pollutants, including nitrogen oxides (NO_x), sulfur dioxide (SO_2), carbon monoxide (CO), and particulate matters (PMs). NO_x and PMs are to a certain extent related to nearly 450,000 premature deaths in Europe [2]. Particularly, in the urban atmosphere, NO_x count as one of the most common gaseous pollutants, which are very harmful to human health. Adverse environmental effects (like acid rain and ozone depletion) can be caused toward the NO_x Earth's atmosphere release [3].

However, the reduction of atmosphere pollutants cannot only be mitigated by active reduction of the emissions but also needs to be mitigated by novel technologies and materials. During the last two decades, novel multifunctional building materials (belonging to the so-called passive reduction techniques) have been designed by embedding photocatalysts, in a large number of surfaces, employed to reduce (oxidize) the pollutants via photocatalytic reaction (PCR) [4, 5]. Photocatalysts, for example, TiO_2 , are using UV light to convert adsorbed water and oxygen into highly reactive radicals (OH , O_2^-) which oxidize adsorbed pollutants. For example, NO_x is oxidized to NO_3^- , which stays on the surface until rainwater may successfully clean it [6]. Another effect of PCR is the hydrophilic behavior of water on irradiated surfaces. In combination with the oxidation process of the PCR, organic and inorganic substances are prevented from sticking to the surface, which leads to their self-cleaning effect. Self-cleaning of these materials will also prevent blocking of active sites of the catalyst by pollutants (i.e., “urban grime”), prolonging its photocatalytic activity for many years [7, 8]. These two fundamental surface photochemical properties of photocatalysts have been extensively studied in a number of publications [9–11].

The application of TiO_2 photocatalysts to the construction materials started toward the end of the 1980s [8]. To improve the practical applications of TiO_2 photocatalysts, among several supporting materials, the cement-based materials are of

great interest due to their strong binding property and porous structures. In recent years, several photocatalytic cementitious materials have been developed and patented by researchers all over the world [12–15]. The great advantage of developing photocatalytic cementitious materials is that the only requirements, beyond TiO₂ in the construction material used, are sunlight, oxygen, and water [16]. Besides, immobilizing the powdered photocatalysts into the cement matrix provides surfaces that can be reached by light irradiation. The irradiation of the surface with solar/UV light with a wavelength <400 nm leads to a photo-induced oxidation of the compounds absorbed on cement surface caused by TiO₂ [17].

There are generally two kinds of methods to combine TiO₂ with cementitious composites: (i) incorporation into the cement matrix during mixing process and (ii) coating TiO₂ on the surface of cement specimens by using spray pyrolysis techniques [18, 19]. However, many researches have shown that these methods still have critical problems for long-term applications like agglomeration of TiO₂ particles in the cement matrices, blockage of TiO₂ particles by cement hydrates, and adhesion and abrasion between the TiO₂ and cement surface, resulting in low photocatalytic efficiencies [8, 20–22]. Above all, by mixing the TiO₂ into the cement matrices, most of TiO₂ will be placed deeply inside the cement hydration products, so that little UV light can pass through the composite to activate the TiO₂.

Adjusting the microstructure of cement matrix and introducing pores into the matrix could be an effective method to build up one interconnected structure for TiO₂ photocatalysis and to improve the dispersion and exposure degrees of TiO₂ particles in cement matrix [23]. In this direction, highly porous TiO₂-modified cement-based foams present a micro- to meso-structure, which can be beneficial for photocatalytic efficiency and TiO₂ utilization. A continuous uniform pore structure can allow the UV light to go deeper inside into the porous foam to activate TiO₂. Therefore, the corresponding foam composite enhances the reactants and light diffusion depth, resulting in better photo-cleaning performance [24–27].

In this study, the effects of the photocatalytic performance of highly porous TiO₂ cementitious foams are evaluated. The study is thus also investigating the interaction between TiO₂ powders, the cementitious hosting environment, and their consequences on the conventional properties of the material, such as rheology, thermal and mechanical resistance, or durability. In this sense, the proposed highly porous cementitious composite represents a novel breakthrough insulation system that will replace available insulation materials with multifunctional energy-saving and air-cleaning performances. Current activities at the WiB TU Darmstadt deal with developing a novel translucent PCM-TiO₂-glass fiber-reinforced cementitious foam as further extension of the *foam* to possibly enhance photocatalyst components for better air cleaning in combination with energy saving. It is important to highlight that insulation materials are not directly exposed to external environment. To achieve a multifunctional behavior (insulator and photocatalyst) for the highly porous TiO₂ cementitious foams, UV exposure is necessary, and also air flowing should be allowed. For this purpose, a translucent external plaster will be needed in practical applications.

2.2 Materials and Methods

This section deals with the materials and related preparation of the TiO₂-foamed concrete samples. Then, methods for testing the NO_x reduction efficiency, through photocatalytic activity, and for characterizing thermal and mechanical properties are shown.

2.2.1 Materials

Raw Material For the cement paste, an ordinary *Portland cement* (i.e., type 52.5 by the Heidelberg Cement AG, Germany) together with two types of chemical additives, namely, *Melamine resin sulfonate* as stabilizer (i.e., Sika ST 3, $\rho = 1070 \text{ kg/m}^3$) and *chloride-free hardening accelerator* (i.e., DARASET 304, $\rho = 3000 \text{ kg/m}^3$), were used. In addition, a *protein-based foaming agent* (i.e., Pantapor FA by Ha-Be Betonchemie GmbH & Co. KG, Germany) was chosen in order to reach higher stability with more favorable thermal and mechanical characteristics [28, 29]. TiO₂ photocatalyst ($\rho = 3900 \text{ kg/m}^3$) KRONO Clean-7050 was provided by the KRONOS International, Inc.

2.2.2 Mixture Design and Sample Preparation

Foamed concrete samples were prepared with three different porosities, 54%, 77%, and 88% (meaning the ratio between the aqueous foam volume to 1 m³), and three different amounts of TiO₂ powder of 0 V.-%, 5.0 V.-%, and 10.0 V.-% in substitution of the used Portland cement, as shown in Table 2.1. Aqueous foam with the density of 60 kg/m³ was prepared by using a pre-foaming method. A stabilizer was used to prevent aggregate sedimentation in the fresh state of the cement paste as well as surface bleeding. The hardening accelerator causes an acceleration of the reactions of the cement and thus of the hardening process of the fresh paste. This results in the acceleration of the foam structure formation and the improvement of the pore size stability.

Production of the Porous TiO₂-Cementitious Foam The preparation and mixing of the TiO₂ cementitious foam can generally be divided into three steps: (i) preparation of the TiO₂ cement paste, (ii) production of the aqueous foam, and (iii) mixing the generated foam thoroughly with the TiO₂ cement paste mixture. Figure 2.1 shows the basic principle of foam production.

The TiO₂ cementitious foam was prepared at 20 °C and following the proportions listed in Table 2.1. In order to prepare the foam with homogeneous pores, water and the half amount of Portland cement were firstly poured into a colloidal mixer. After

Table 2.1 Overview of mixture proportions in 1 m³ cementitious foam with three different TiO₂ contents and three different porosities

Labels	f-54-ref	f-54-5%	f-54-10%	f-77-ref	f-77-5%	f-77-10%	f-88-ref	f-88-5%	f-88-10%
	[kg/m ³]								
Cement	597.00	565.00	534.00	299.00	282.00	267.00	150.00	143.00	135.00
Water	248.30	249.95	251.83	124.38	124.75	125.92	62.40	63.26	63.67
Stabilizer	11.94	11.30	10.68	5.98	5.64	5.30	3.00	2.86	2.70
TiO ₂	–	37.29	74.23	–	18.61	37.11	–	9.44	18.80
Hardening accelerator	23.88	22.60	21.36	11.96	11.28	10.68	6.00	5.72	5.40
Aqueous foam	32.40	32.41	32.39	46.17	46.23	46.19	53.06	53.01	53.01

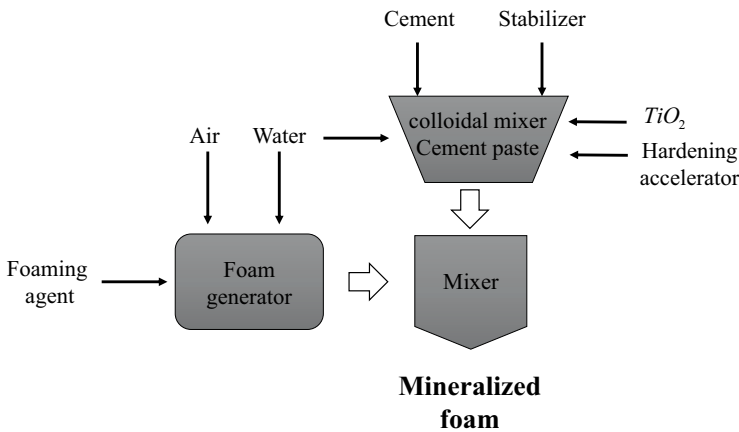


Fig. 2.1 Production of TiO₂ mineral foam – mixing scheme

stirring them for 60 s at a speed of approximately 1300 U/min, the other half of the cement was poured into the colloidal mixer followed by another 60 s stirring. Next, the stabilizer was added and mixed at a low speed. After 30 s, TiO₂ particles were slowly dispersed into the fresh paste for 30 s. Finally, the hardening accelerators were poured into the mixture for 30 s as well. Lastly, the speed was increased to about 5000 U/min for another 30 s until complete homogenization was achieved.

The aqueous foam was produced using a foam generator (Fig. 2.2) to the aimed 60 kg/m³ density. The generator is equipped with a proportional mixer to add a fixed amount of foaming agent (i.e., 2%) to the water. Using compressed air flowing into the fluid, the kinetic energy is converted into surface energy. The generated cementitious foam was then thoroughly mixed with the paste mixture and poured into a mold (600 mm³) and left for one/two days in an air-conditioned room (20 °C). Then, samples were fully covered with polyethylene film and cured at 20 °C until 28 days. After that, all specimens were oven dried at 45 °C until constant weight was achieved.

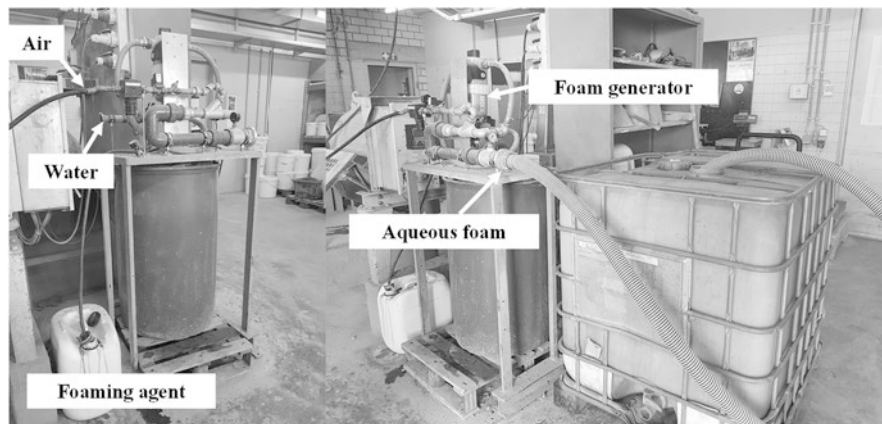


Fig. 2.2 Experimental setup for the foam generator at the TU-Darmstadt

For each mixture, two samples (9.9 cm \times 4.9 cm \times 2.0 cm) were prepared for the photocatalytic tests. The experimental program was then completed for evaluating physical (e.g., specific weights and dry densities), thermal, and mechanical properties of the considered cementitious foams. These latter have been omitted in this paper for the sake of brevity.

2.2.3 Methods

Photocatalytic Tests Experiments on the considered TiO₂ cementitious foams were carried out in collaboration with the Atmospheric and Environmental Research (AER) Institute of the University of Wuppertal. For the evaluation of air purification efficiency, titanium dioxide powder (TiO₂, Kronos) added with 5% and 10% in substitution of the cement powder was considered. The reactivity of NO_x (NO+NO₂) degradation and the side products, nitrous acid (HONO) and formaldehyde (HCHO), were investigated by measuring the photocatalytic deposition rate.

Prior to the experiments, samples were rinsed with high purity water, dried, and activated for several days with a fluorescent lamp at 33 W m⁻² UVA light. This pre-treatment serves to oxidize possible organic impurities by the self-cleaning effect of photocatalysis to achieve higher activity and better reproducibility of the results.

The photocatalytic activity of the samples was evaluated close to the reaction conditions specified in the ISO 22197-1 (2007), that is, 10 W m⁻² UVA, 40% relative humidity, and 20 °C in a temperature-controlled Photo Flux reactor; see Fig. 2.3. NO and NO₂ were used as reactants.

A chemiluminescence meter (Ansyco AC 31M with molybdenum converter, 2 ppb detection limit) was used to determine the concentration of nitrogen oxide (NO_x = NO + NO₂). The reactant concentration (NO+NO₂) was adjusted from the

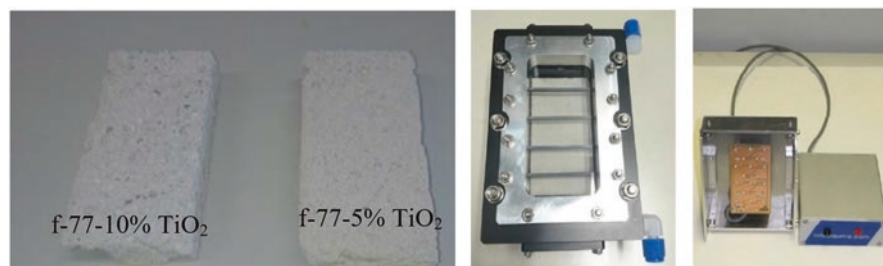


Fig. 2.3 Left: Open-pore cementitious foam specimens with 5% and 10% TiO₂ content (77% porosity). Middle: Flux reactor for the determination of photocatalytic activity. Right: Adjustable diode array with intensity control (QUMA-Elektronik & Analytik, Wuppertal) as UVA light source ($\lambda_{\max} = 370$ nm; $\Delta\lambda \pm 20$ nm)

ISO standard of 1 ppm to approximately 50 ppb and 100 ppb in respect of the typical environmental concentration. Inside the reactor, the distance between the specimen and the glass is about 1–2 mm (contrary to the suggested ISO value of 5 mm) to guarantee a turbulent airflow. The chemiluminescence meter was previously calibrated with NO gas for each test.

NO₂ concentration was calculated from the difference between the NO₂ signal of the chemiluminescence device (NO_y-NO) and the measured HONO concentration. For this purpose, a highly sensitive and selective HONO-LOPAP measuring device with a detection limit of 5 ppt was used (see Heland et al. (2001) [30], Kleffmann et al. (2002) [31]). Formaldehyde (HCHO) was determined with a sensitive formaldehyde monitor (AL 4021) from the company AERO LASER (detection limit 50 ppt), which is based on the so-called Hantzsch method. Both the formaldehyde and the LOPAP measuring device were regularly calibrated. Figure 2.4 illustrates a scheme of the experimental setup. Bottles with NO or NO₂ gases are diluted together with synthetic air. A flow controller (Brooks thermal mass flow controller) is used to control the desired concentration of the pollutant gas, either NO or NO₂ in synthetic air.

The mixed gas flows through a humidified coil to the NO_x, HONO, and HCHO reference sensors. This process is called a bypass, whereby the gas flow is not yet connected to the reactor. This allows the reference sensors to be calibrated. The gas stream can also be connected to the reactor to analyze the photocatalytic performance.

For the samples, the self-emissions of NO, NO₂, HONO, and HCHO were first investigated. For this purpose, after daily calibration of the NO_x measuring instrument (zero, span, zero), humidified (40% r.h.) synthetic air was passed over the samples, and their self-emissions were measured first in the dark and then under UVA irradiation (10 W m⁻²) and finally again in the dark. Then, the reactions with the reactants ((1) NO₂ and (2) NO) were carried out at two concentrations each of approximately 50 ppb and 150 ppb, respectively. A measurement includes the following sequence: zero/bypass, NO_x/bypass, NO_x/reactor dark, and NO_x/reactor UV.

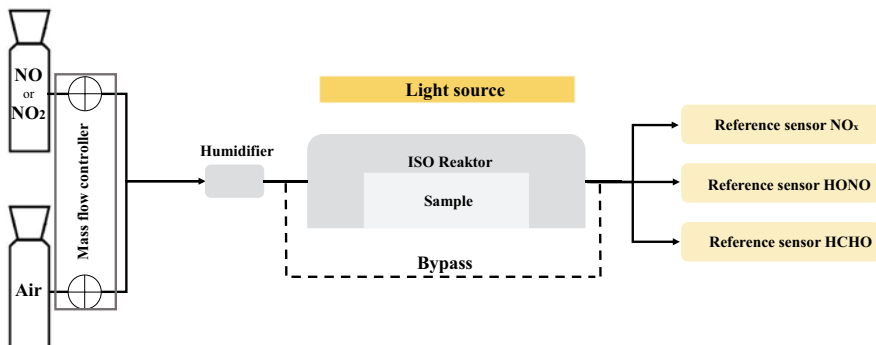


Fig. 2.4 Illustration of the experimental setup

Mechanical and Thermal Tests

Mechanical and thermal tests are also performed on the considered foam mixtures. On one hand, the mechanical tests of the samples are tested according to the procedures described in EN 196-1. For each mixture, nine prisms (40 mm × 40 mm × 160 mm) are tested under both three-point bending and compression. The obtained peak stress of compressive strengths ranged between 0.22 and 0.28 MPa. On the other hand, thermal conductivities were measured through the guarded hot plate method [32] for the considered mixture on three temperature levels (i.e., 10, 25, and 40 °C). Subsequently, the thermal conductivity of the dry material at 10 °C is extrapolated. These tests are carried out according to both DIN EN 12667:2001 and ISO 8302:1991-08.

2.3 Results and Discussion

2.3.1 Photocatalytic Activity

The evaluation of photocatalytic activity (ν_{Photo}) was made by deposition velocity:

$$\nu_{\text{Photo}} = \frac{\ln\left(\frac{c_{t=0}}{c_t}\right) \cdot J_{\text{gas}}}{S} \quad (2.1)$$

being $c_{t=0}$ and c_t the reactant concentration [ppb] at the input and output, respectively, J_{gas} the total flux [cm^3/s], and S the active surface [cm^2]. The photocatalytic deposition velocity (ν_{Photo}) in [cm/s] does not contain transport resistances because of the turbulent flow conditions. The deposition velocity refers to the total degradation between input and output values. More details of the different kinetic evaluations to ISO 22197-1 can be found in [33].

Besides the kinetic evaluation, the formation of the side products was investigated. The emission flux of formaldehyde E_{HCHO} [molecules/(cm² × s)] was calculated with the volume flux (Φ_{gas}^{ϕ} , cm³/s, at 298 K, 1 atm), the active surface (S , [cm²]), and the HCHO concentration (ppb):

$$E_{\text{HCHO}} = \frac{([\text{HCHO}]_{\text{Photo}} - [\text{HCHO}]_{\text{Dunkel}}) \cdot 2.46 \times 10^{10} \text{ cm}^{-3} \text{ ppb}^{-1} \cdot \Phi_{\text{gas}}^{\phi}}{S} \quad (2.2)$$

In the following, the photocatalytic results of the f-77-5% and f-77-10% mixtures have been reported. They represent the optimum combination of acceptable mechanical and thermal performances together with excellent NO_x cleaning.

Results on NO_x In the dark, the samples show no activity against NO. Contrarily with NO₂, they showed a clear reaction under dark conditions which can be caused by the reaction of NO₂ with water to HONO and nitrate, that is, $2 \text{NO}_2 + \text{H}_2\text{O} \rightarrow \text{HONO} + \text{HNO}_3$. This could also explain the formation of HONO (however, quite low) under the same dark conditions. On the other hand, under UV irradiation, the samples show significant photocatalytic activity with both NO and NO₂. The observed NO and NO₂ degradation rates of both specimens under UV irradiation were $\nu(\text{NO})_{\text{Photo}} = 0.48 \text{ cm/s}$ and $\nu(\text{NO}_2)_{\text{Photo}} = 0.55 \text{ cm/s}$, respectively, which clearly exceeded the limit for the deposition velocity of $\geq 0.1 \text{ cm/s}$ proposed in the literature (see, for example, Ifang et al. (2014) [33]), at which an improvement in air quality can still be expected. More details on the photocatalytic activity of the samples and the photocatalytic deposition rates can be seen in Fig. 2.5 and Table 2.2.

As shown in Table 2.2, the degradation of NO_x of the specimen with 5% TiO₂ exceeded the degradation performance of the specimen with 10% TiO₂. This could be explained by the better foam structure of the specimen achieved with the 5% amount of TiO₂. The hydrophilic behavior of water in contact with TiO₂ could be a reason for the damage of the foam structure during casting, which is much more evident in the 10% TiO₂ concrete foams.

The reaction of NO to nitrate is proceeding by the intermediate step of NO₂: $\text{NO} \rightarrow \text{NO}_2 \rightarrow \text{HNO}_3/\text{nitrate}$. The intermediate NO₂ was observed in the experiments with around 10–33% which can be explained by the short residence time in the reactor (~0.3 s). Due to that, no complete degradation to nitrate can take place.

It is worth mentioning that values of 0.50 cm/s ca. of deposition velocities for NO and NO₂ were observed for concrete samples in [34] and values in the range of 0.03–0.60 cm/s were achieved by Boonen et al. (2017) [35] for different cementitious materials on pavement blocks. Contrarily, values of up to 1.06 cm/s of deposition velocities for NO and NO₂ can be observed in this experimental campaign, shown to be the high potential of the tested TiO₂ porous cementitious composites.

Results on Nitrous Acid (HONO) Due to the alkaline cement, the formation of HONO during active photodegradation of NO₂ is around ~0.3 %, which is significantly below the limit value of 5% required (see Ifang et al. (2014) [33]). Also, the

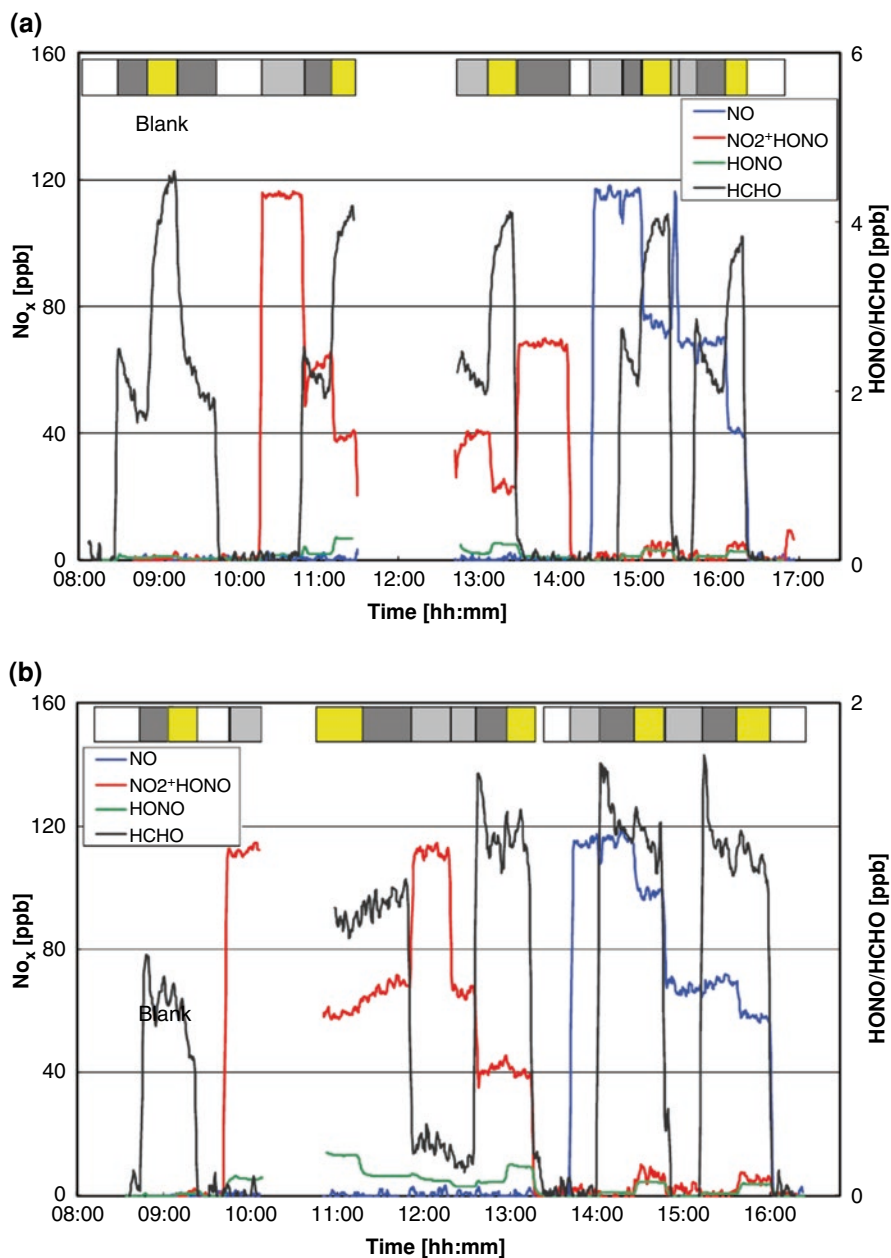


Fig. 2.5 Concentration-time curve for the reaction of NO_2 or NO for the sample (a) with 5% TiO_2 and (b) with 10% TiO_2 . The bars drawn at the top indicate the times for zero (white), NO_x -bypass (light gray), reactor dark (dark gray), and reactor + light (yellow). At the beginning of the experiment (blank), the humidity was lower than toward the end

Table 2.2 Photocatalytic deposition velocities [cm s^{-1}] of the investigated samples against NO, NO₂, and HONO. The data refer to relative humidity of 40% and radiation intensity of 10 W m^{-2}

Mixture	$\nu(\text{NO})_{\text{Dunkel}}$	$\nu(\text{NO})_{\text{Photo}}$	$\nu(\text{NO}_2)_{\text{Dunkel}}$	$\nu(\text{NO}_2)_{\text{Photo}}$	$\nu(\text{HONO})_{\text{Photo}}$
f-77-5%	<0.007	0.48 ± 0.11	0.54 ± 0.12	1.06 ± 0.20	See Fig. 2.5
f-77-10%	<0.006	0.15 ± 0.04	0.46 ± 0.15	0.55 ± 0.16	See Fig. 2.5

Table 2.3 Photocatalytic HCHO emission flux [$\text{molecules cm}^{-2} \text{ s}^{-1}$] as well as equivalent concentration of NO₂

Mixture	E (HCHO) [$\text{molecules cm}^{-2} \times \text{s}^{-1}$]	NO ₂ [equivalent concentration ppb]
f-77-5%	$(9.9 \pm 2.3) \times 10^{10}$	3.8
f-77-10%	$(3.2 \pm 2.3) \times 10^{10}$	2.3

HONO formation of ~0.4 % during dark conditions is significantly below the theoretical expected value (50 %), which can be explained by the very strong adsorption of HONO on the alkaline cement surface.

Results on Formaldehyde (HCHO) The formation of HCHO emissions from the samples cannot be neglected. This is due to the much more harmful impacts of HCHO than the nitrogen oxides on health. The average formation of HCHO can be considered similar to the deposition flux of NO₂; see Table 2.3. This formation can also come from the photocatalytic degradation of organic binders or additives which could be, for example, the foam agent in this case.

To verify if there is a decrease in HCHO formation with time, further long-term investigations on the specimen or the additives themselves should be conducted.

2.4 Conclusions

This chapter presented the preliminary results of an experimental study which investigated the photocatalytic performance of highly porous cementitious foams enhanced with TiO₂ powders. Several porous structure ratios (i.e., 54%, 77%, and 88%) together with TiO₂ powder fractions (i.e., 0, 5, and 10% in substitution of cement powders) were pretested and analyzed. The results confirmed that the photocatalytic activity measured in terms of NO and NO₂ degradation, under UV irradiations, reached excellent performances when compared to TiO₂ concrete substrate data, available in scientific literature. Moreover, the generation of other air pollutants (like nitrous acid, HONO, and formaldehyde, HCHO) was quite low which makes this new material a very appealing multifunctional composite for photocatalyst air cleaning and building envelope/energy-saving solutions in the field of the construction and building materials. Further investigations are however required to study the possible side effects generated by the other pollutants (i.e., HONO and HCHO) when this material is employed.

Acknowledgments Part of this work has been financed by the EU H2020 NRG-STORAGE project (n° 870114, <https://nrg-storage.eu/>) under the LC-EEB-01-2019 call, H2020-NMBP-ST-IND-2018-2020/H2020-NMBP-EEB-2019, IA type.

References

1. T.D. Pham, B.K. Lee, Feasibility of silver doped TiO₂/glass fiber photocatalyst under visible irradiation as an indoor air germicide. *Int. J. Environ. Res. Pub. Health* **11**, 3271–3288 (2014)
2. Agency, European Environment. Air Quality in Europe: 2020 Report. LU: Publications Office, 2020. <https://data.europa.eu/doi/10.2800/786656>. Last accessed 21 July 2021.
3. S. Manahan, *Environmental chemistry* (CRC Press, Boca Raton, 2017)
4. M. Malayeri, H. Fariborz, L. Chang-Seo, Modeling of volatile organic compounds degradation by photocatalytic oxidation reactor in indoor air: A review. *Build. Environ.* **154**, 309–323 (2019)
5. A. Talaiekhosani, S. Rezaia, K.H. Kim, R. Sanaye, A.M. Amani, Recent advances in photocatalytic removal of organic and inorganic pollutants in air. *J. Clean. Prod.* **278**, 123895 (2020)
6. V. Binas, D. Venieri, D. Kotzias, G. Kiriakidis, Modified TiO₂ based photocatalysts for improved air and health quality. *J. Materiomics* **3**(1), 3–16 (2017)
7. J. Chen, S.C. Kou, C.S. Poon, Photocatalytic cement-based materials: Comparison of nitrogen oxides and toluene removal potentials and evaluation of self-cleaning performance. *Build. Environ.* **46**(9), 1827–1833 (2011)
8. A. Folli, C. Pade, T.B. Hansen, T. De Marco, D.E. Macphee, TiO₂ photocatalysis in cementitious systems: Insights into self-cleaning and depollution chemistry. *Cem. Concr. Res.* **42**(3), 539–548 (2012)
9. A. Fujishima, K. Hashimoto, T. Watanabe, *TiO₂ photocatalysis: Fundamentals and applications* (BKC Inc, Tokyo, 1999)
10. A.G. Agrios, P. Pichat, State of the art and perspectives on materials and applications of photocatalysis over TiO₂. *J. Appl. Electrochem.* **35**, 655e63 (2005)
11. A. Fujishima, X. Zhang, D.A. Tryk, TiO₂ photocatalysis and related surface phenomena. *Surf. Sci. Rep.* **63**, 515e82 (2008)
12. R. Cucitore, S. Cangiano, L. Cassar, High durability photocatalytic paving for reducing urban polluting agent, WO/2006/000565 (2006)
13. Y. Murata, H. Tawara, H. Obata, K. Murata, NO_x-Cleaning Paving Block, EP0786283 (2003)
14. L. Cassar, A. Beeldens, N. Pimpinelli, G.L. Guerrini, Photocatalysis of cementitious materials, in *International RILEM Symposium on Photocatalysis, Environment and Construction Materials, RILEM, Florence*, ed. by L. Cassar, P. Baglioni, (2007), pp. 131–145
15. G.L. Guerrini, A. Plassais, C. Pepe, L. Cassar, Use of photocatalytic cementitious materials for self-cleaning applications, in *International RILEM Symposium on Photocatalysis, Environmental and Construction Materials, RILEM, Florence*, ed. by L. Cassar, P. Baglioni, (2007), pp. 219–226
16. T. Meng, Y. Yu, X. Qian, S. Zhan, K. Qian, Effect of nano-TiO₂ on the mechanical properties of cement mortar. *Constr. Build. Mater.* **29**, 241–245 (2012)
17. M. Pérez-Nicolás, J. Balbuena, M. Cruz-Yusta, L. Sánchez, I. Navarro-Blasco, J.M. Fernández, J.I. Alvarez, Photocatalytic NO_x abatement by calcium aluminate cements modified with TiO₂: Improved NO₂ conversion. *Cem. Concr. Res.* **70**, 67–76 (2015)
18. C. Cárdenas, J.I. Tobón, C. García, J. Vila, Functionalized building materials: Photocatalytic abatement of NO_x by cement pastes blended with TiO₂ nanoparticles. *Constr. Build. Mater.* **36**, 820–825 (2012)
19. C. Mendoza, A. Valle, M. Castellote, A. Bahamonde, M. Faraldos, TiO₂ and TiO₂-SiO₂ coated cement: comparison of mechanic and photocatalytic properties. *Appl. Catal. B* **178**, 155–164 (2015)

20. M. Lackhoff, X. Prieto, N. Nestle, F. Dehn, R. Niessner, Photocatalytic activity of semiconductor-modified cement – Influence of semiconductor type and cement ageing. *Appl. Catal. B* **43**(3), 205–216 (2003)
21. F. Chen, X. Yang, H.K.C. Mak, D.W.T. Chan, Photocatalytic oxidation for antimicrobial control in built environment: A brief literature overview. *Build. Environ.* **45**, 1747–1754 (2010)
22. J. Chen, C.S. Poon, Photocatalytic construction and building materials: From fundamentals to applications. *Build. Environ.* **44**(9), 1899–1906 (2009)
23. W. Qiu, Y. Zheng, A comprehensive assessment of supported titania photocatalysts in a fluidized bed photoreactor: Photocatalytic activity and adherence stability. *Appl. Catal. B* **71**, 151–162 (2007)
24. J. Chen, C.S. Poon, Photocatalytic cementitious materials: Influence of the microstructure of cement paste on photocatalytic pollution. *Environ. Sci. Technol.* **43**, 8948–8952 (2009)
25. R. Sagrañez, J.I. Álvarez, M. Cruz-Yusta, I. Mármol, J. Morales, J. Vila, L. Sánchez, Enhanced photocatalytic degradation of NO_x gases by regulating the microstructure of mortar cement modified with titanium dioxide. *Build. Environ.* **69**, 55–63 (2013)
26. J. Chen, S.C. Kou, C.S. Poon, Hydration and properties of nano-TiO₂ blended cement composites. *Cem. Concr. Compos.* **34**(5), 642–649 (2012)
27. E. Jimenez-Relinque, J.R. Rodriguez-Garcia, A. Castillo, M. Castellote, Characteristics and efficiency of photocatalytic cementitious materials: type of binder, roughness and microstructure. *Cem. Concr. Res.* **71**, 124–131 (2015)
28. A. Gilka-Bötzow, S. Yang, & E.A. Koenders, Ultralight Mineral Foams for Sustainable Insulation Applications
29. M. Hashim, M. Tantray, Comparative study on the performance of protein and synthetic-based foaming agents used in foamed concrete. *Case St. Constr. Mater.* **14**, e00524 (2021)
30. J. Heland, J. Kleffmann, R. Kurtenbach, P. Wiesen, A new instrument to measure gaseous nitrous acid (HONO) in the atmosphere. *Environ. Sci. Technol.* **35**, 3207–3212 (2001)
31. J. Kleffmann, J. Heland, R. Kurtenbach, J.C. Lörzer, P. Wiesen, A new instrument (LOPAP) for the detection of nitrous acid (HONO). *Environ. Sci. Pollut. Res.* **9**, 48–54 (2002)
32. A. Gilka, P. Folino, A. Maier, E.A. Koenders, A. Caggiano, Triaxial failure behavior of highly porous cementitious foams used as heat insulation. *Processes* **9**, 1373 (2021)
33. S. Ifang, M. Gallus, S. Liedtke, R. Kurtenbach, P. Wiesen, J. Kleffmann, Standardization methods for testing photo-catalytic air remediation materials: Problems and solution. *Atmos. Environ.* **91**, 154–161 (2014)
34. F. Mothes, S. Ifang, et al., Bed flow photoreactor experiments to assess the photocatalytic nitrogen oxides abatement. *Appl. Catal. B: Environ.* **231**, 161–172 (2018)
35. E. Boonen, A. Beeldens, I. Dirckx, V. Bams, Durability of cementitious photocatalytic building materials. *Catal. Today* **287**, 196–202 (2017)